CFD simulation of heat and mass transfer processes in a metal hydride hydrogen storage system, taking into account changes in the bed structure

Konstantin B. Minko [a], Mykhaylo V. Lototskyy [b,c,*], Irina E. Bessarabskaya [d], Boris P. Tarasov [c,e,**]

[a] National Research University "Moscow Power Engineering Institute" (MPEI), Moscow, Russian Federation
[b] HySA Systems Competence Centre, South African Institute for Advanced Materials Chemistry (SAIAMC), University of the Western Cape, Bellville, South Africa
[c] Federal Research Center of Problems of Chemical Physics and Medicinal Chemistry RAS, Chernogolovka, Russian Federation
[d] Moscow Institute of Radio Engineering, Electronics, and Automation, Russian Technological University, Moscow, Russian Federation
[e] National Research University Higher School of Economics, Moscow, Russian Federation

ARTICLE INFO

ABSTRACT

CFD modelling of heat-and-mass transfer in metal hydride (MH) beds is an important step in the development and optimisation of MH reactors for hydrogen storage, compression and separation/purification. In the existing models, the mass conservation equation includes the density of solid in the non-hydrogenated (ρ_s) and hydrogen-saturated (ρ_{ss}) states. To provide constant porosity of the MH bed during H_2 absorption/desorption, assumption $\rho_s < \rho_{ss}$ is typically taken. However, this assumption contradicts to well-known fact that hydrogenation of hydride-forming alloys is accompanied by the expansion of crystal lattice of the metallic matrix and, therefore, by the decrease of the solid density by 15–25%.

This work presents results of the modelling which takes this effect into account. The model assumes that the density of the MH changes linearly as the starting hydride-forming alloy is saturated with hydrogen, while the volume of the MH bed remains constant. The last assumption is a limiting estimation because it provides the maximum possible reduction in the porosity during H_2 absorption process.

The model was validated using published experimental data on a cylindrical MH reactor filled with 422 g of $LaNi_5$. It was shown that accounting the realistic changes in the MH density can significantly affect the simulation results.

1. Introduction

Hydrogen storage is a key enabling technology for the advancement of hydrogen fuel cell power systems in transportation, stationary, and portable applications [1–7]. Metal hydrides (MH) offer a promising alternative to other H_2 storage technologies including both conventional (compressed gas and cryogenic liquid) and newly developed (e.g., Liquid Organic Hydrogen Carriers/LOHC) ones [8–10]. Main advantages of the MH H_2 storage technology include very high hydrogen storage density per unit volume (equivalent to the storage of compressed H_2 up to 800–1000 bar), low storage pressures (below ~10 bar), modest consumption of energy in the form of low-grade heat, as well as technological flexibility which allows efficient integration of the MH H_2

storage component into BoP of the hydrogen fuel cell power systems [11–14].

Main problem of MH technologies for hydrogen storage and related applications (e.g., hydrogen compression and heat management, hydrogen separation and purification) is in the decrease of the hydrogen charge and discharge rates when upscaling the metal hydride reactors. Despite the intrinsic (isothermal) kinetic of hydrogenation/dehydrogenation of hydride forming intermetallics, as a rule, is very fast, a combination of poor effective thermal conductivity of the MH bed (below 1 W/(m K) for the powders) and relatively high heat effects of hydride formation (exo-) and decomposition (endo-) varying between 20–25 and 35–40 kJ/mol H_2 results in a quick approach of the MH bed temperature to its equilibrium value and virtual stop of the reaction further rate-limited by the heat transfer in the MH bed. Thus, the acceleration of

* Corresponding author. HySA Systems Competence Centre, South African Institute for Advanced Materials Chemistry (SAIAMC), University of the Western Cape, Bellville, South Africa.
** Corresponding author. Federal Research Center of Problems of Chemical Physics and Medicinal Chemistry RAS, Chernogolovka, Russian Federation.
E-mail addresses: mlototskyy@uwc.ac.za (M.V. Lototskyy), tarasov@icp.ac.ru (B.P. Tarasov).

Nomenclature

A	specific surface area, m^2/m^3
c_p	specific heat capacity, J/(kg·K)
k	permeability, m^2
$\dot{m}$	source of hydrogen absorption/desorption per unit volume, kg/(m^3 s)
M	molar mass, kg/mol
t	time, s
T	temperature, K
X	hydrogen-saturated fraction of the alloy
$\overline{X}$	number of H atoms per formula unit of the alloy
w	velocity, m/s

Greek symbols

α	heat transfer coefficient, W/(m^2K)
ΔH	hydrogenation/dehydrogenation enthalpy, J/kg H_2
λ	thermal conductivity, W/(m·K)
ρ	density, kg/m^3

φ	porosity of the MH bed

Superscripts

*	effective properties

Subscripts

a	absorption
d	desorption
eff	effective properties
g	gas phase
H	monatomic hydrogen
s	solid phase
s0	alloy non-saturated with hydrogen
sg	solid–gas interphase
ss	alloy saturated with hydrogen

Abbreviations

MH	metal hydride

the latter process, first of all, via increase of the effective thermal conductivity of the MH bed, is essential for the development of the MH reactors with good dynamic performance [14–16]. The optimisation of the reactor design requires numerical modelling (as precise as possible) of heat-and-mass transfer in the MH beds. Forecasting of dynamic performances of MH beds having pre-set geometry and dimensions, as well as influence of the operating conditions on the hydrogen charge/discharge dynamics is also very important outcome from the modelling [17,18].

Computational Fluid Dynamic (CFD) is a useful and convenient tool for the modelling of MH reactors for hydrogen storage, compression, and purification [18–23].

In most numerical studies, the properties of the MH bed including porosity, effective thermal conductivity (ETC) and permeability, are assumed to be constant and not depending on the hydrogen concentration in the solid, or the fraction of the hydrogen storage alloy (X) saturated with hydrogen [24]. In the existing models, the mass balance governing equation includes the density of solid in the non-hydrogenated (ρ_s) and hydrogen-saturated (ρ_{ss}) states. To provide constant porosity of the MH bed during H_2 absorption/desorption processes, assumption $\rho_s < \rho_{ss}$ is typically taken, for example, $\rho_s = 8400$ and $\rho_{ss} = 8520$ kg/m^3 for LaNi$_5$ [25]. However, this assumption contradicts to well-known fact that hydrogenation of hydride-forming alloys is accompanied by the expansion of crystal lattice of the metallic matrix [26] and, in turn, by the decrease of the solid density by 15–25%. For the AB$_5$-type alloys typical value of ρ_s varies between 8200 and 8400 kg/m^3 while their hydrides, AB$_5$H$_{\sim6}$ are characterised by $\rho_{ss} = 6300$–6800 kg/m^3 [27]. At a fixed MH bed volume (with no free space above the bed), this change in density will lead to a noticeable decrease in the MH bed porosity, which means an increase in the ETC and a decrease in permeability. Evaluation of the effect of changing the ETC on the process of heat and mass transfer in MH hydrogen storage systems has not been studied enough. In the literature [28], this effect was discussed regarding determination of the ETC of the MH beds. However, in the numerical simulation of heat and mass transfer processes in MH systems, these results were seldom used.

Mellouli et al. [29] modelled hydrogen absorption/desorption taking into account the deformation of the MH bed and concluded that this factor practically does not influence on the calculation results. The authors used the additive model for the estimation of the effective thermal conductivity of the MH bed:

$$\lambda_{eff} = (1 - \varphi)\lambda_s + \varphi\lambda_g \qquad (1)$$

where φ is a porosity of the MH bed, λ_s is an effective thermal conductivity of the solid phase assumed to be of 3.18 W/(m K), i.e., far below the true thermal conductivity of the MH material equal to ~10–15 W/(m K) [30].

Eq. (1) cannot predict real changes of λ_{eff} when changing the bed porosity and thermal conductivity of the gas phase (e.g., hydrogen and gas impurities). This problem has been discussed in the works focused on the development of more precise models of the effective thermal conductivity [28,31]. Matsushita et al. [28] showed that during hydrogen absorption in LaNi$_5$ at $T = 60$ °C and $P \sim 1$ MPa ETC increases in almost two times. Kallweit and Hahne [31] studied changes of ETC of a MH bed of the fixed volume (not accounting the deformation of the containment) and demonstrated that the hydrogen saturation fraction significantly influences on the ETC.

Significant changes of MH bed properties during hydrogen absorption/desorption have been directly confirmed by the measurements of permeability [32] which showed that its value decreases by almost order of magnitude for the hydrogen-saturated alloy. This effect was further analysed in the study [33] which was focused on the changes of permeability but did not discuss the changes of ETC.

This work presents results of numerical studies of the influence of changes of the effective thermal conductivity of the metal hydride bed during hydrogen absorption/desorption on the process of heat and mass transfer in a metal hydride reactor. The cases for which neglecting this effect may result in significant errors of the performance evaluation for the metal hydride systems under development are analysed. Recommendations on the selection of the value of the effective thermal conductivity for the simulation of hydrogen absorption/desorption in metal hydride reactors are presented as well.

2. Materials and methods

2.1. Problem statement

A cylindrical MH reactor containing 422 g of LaNi$_5$ powder and heated/cooled from the outside [34] was simulated in this study (Fig. 1).

We considered two operational modes of the MH reactor, *viz*, (i) hydrogen charge (absorption) at a constant pressure, and (ii) hydrogen discharge (desorption) at a constant flow rate.

In the first case hydrogen pressure at the input was fixed and hydrogen was assumed to enter the reactor at the temperature of 20 °C.

In the second case hydrogen was released from the output at the fixed flow rate, and the desorption took place due to the pressure decrease in

ARTICLE IN PRESS

K.B. Minko et al.   International Journal of Hydrogen Energy xxx (xxxx) xxx
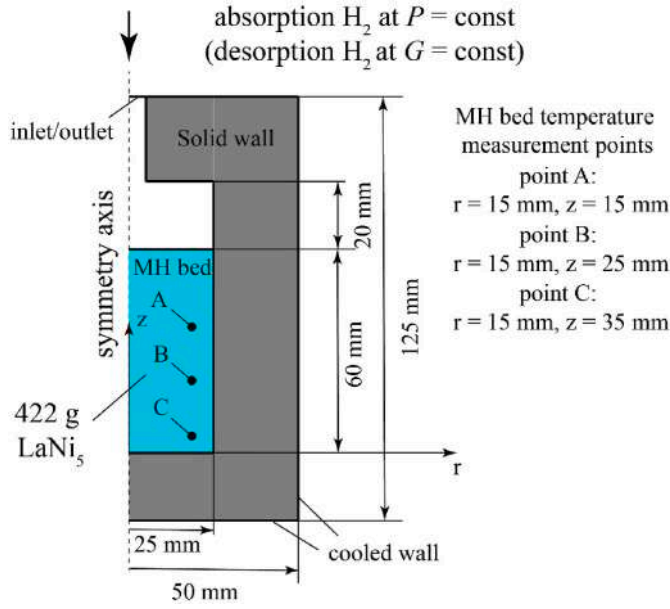

Fig. 1. Configuration of MH reactor [34] simulated in this work.

the reactor. Within such task statement, the calculation was aimed at the determination of hydrogen pressure in the free volume of the reactor. It was assumed that a consumer requires hydrogen at the pressure not lower than 1 bar, and after pressure drop below this value, further operation of the reactor was considered as impractical. The calculation results allow to determine the time of hydrogen supply from the MH reactor to the consumer, as well as the fraction of the alloy saturation with hydrogen which remains in the reactor after the pressure drops below the specified threshold. Similar approach was applied in the experimental study [35].

The coefficient of heat transfer between the reactor wall and the cooling (H_2 absorption) and heating (H_2 desorption) fluid, as well as the temperature of the latter were assumed to be constant.

We assume the densities of $LaNi_5$ and $LaNi_5H_6$ as 8400 and 6800 kg/m^3, respectively [36,37]. It is also assumed that the change between these limiting values is linear as respect to X:

$$\rho_s(X) = \rho_{s0} + (\rho_{ss} - \rho_{s0})\,X \tag{2}$$

We analyse the limiting case when the volume of the MH bed and the filling density, $[1 - \varphi(X)]\,\rho_s(X)$, remain constant. Insignificant increase of the latter (by approximately 1.5%) was not accounted. When using the above assumptions, the porosity at any moment can be determined as:

$$\varphi(X) = 1 - \frac{(1 - \varphi_{s0})\rho_{s0}}{\rho_s(X)} \tag{3}$$

The changes of diameter of MH particles forming the bed are calculated starting from the mass balance equation and the actual density of the alloy.

2.2. Mathematical model

In this work, we used two-temperature model of a porous medium:

$$(1 - \varphi)\,\rho_s\,\frac{d\overline{X}}{dt} = \frac{M_{MH}}{M_H}\dot{m} \tag{4}$$

$$(1 - \varphi)\rho_s c_{p,s}\frac{dT_s}{dt} = \nabla \bullet \left[(1 - \varphi)\lambda_s^*\nabla T_s\right] + \alpha_{sg}A_{sg}\left(T_g - T_s\right)$$
$$+ \dot{m}\left[\Delta H_{sg} + c_{p,H}^s\left(T_{sg} - T_s\right)\right] \tag{5}$$

$$\frac{\partial}{\partial t}\left(\varphi\rho_g\right) + \nabla \bullet \left(\varphi\rho_g\overrightarrow{w_g}\right) = -\dot{m} \tag{6}$$

$$\frac{\partial}{\partial t}\left(\varphi\rho_g w_{g,i}\right) + \nabla \bullet \left(\varphi\rho_g\overrightarrow{w_g} - \varphi\mu_g^*\nabla w_{g,i}\right) = -\varphi(\nabla p)_i - \varphi\frac{\mu_g}{k}w_{g,i}, i = x, y, z \tag{7}$$

$$\varphi\rho_g c_{p,g}\frac{\partial T_g}{\partial t} + \varphi\rho_g\overrightarrow{w_g}c_{p,g}\nabla T_g = \nabla \bullet \left(\varphi\lambda_g^*\nabla T_s\right) + \alpha_{sg}A_{sg}\left(T_s - T_g\right)$$
$$+ \dot{m}c_{p,H_2}^g\left(T_{sg} - T_s\right) \tag{8}$$

The equilibrium pressure was determined from equations presented in Ref. [38]. The value of heat transfer coefficient between the porous medium and gas, α_{sg}, was determined using equation in Ref. [39]. During the calculations the temperature differences did not exceed 0.05 K. The use of the two-temperature model is related to the features of CFD code in which the modelling within this work was done.

The mass source term per unit volume which determines the hydrogen absorption/desorption dynamics, $\dot{m}$, for H_2 absorption and desorption was calculated using equations from Ref. [40]:

$$\dot{m}_a = C_a(1 - \varphi)\rho_s\frac{M_H}{M_{MH}}\overline{X}_{max}\exp\left(-\frac{E_a}{RT}\right)\ln\left(\frac{p_{H_2}}{p_{eq,a}}\right)(1 - X) \tag{9}$$

$$m_d = -C_d(1 - \varphi)\rho_s\frac{M_H}{M_{MH}}\overline{X}_{max}\exp\left(-\frac{E_d}{RT}\right)\frac{p_{eq,d} - p_{H_2}}{p_{eq,d}}X \tag{10}$$

where $C_a = 59.187$ s^{-1}, $E_a = 21.170$ kJ/mol H_2, $C_d = 9.57$ s^{-1}, $E_d = 16.42$ kJ/mol H_2, $\overline{X}_{max} = (H/LaNi_5)_{max} = 6.0$.

The filtration coefficient was determined using equation:

$$k = [1.1205 \bullet \exp(-3.915 \bullet X) + 0.0187] \bullet 10^{-12}\ \text{m}^2 \tag{11}$$

which was derived by the approximation of experimental data [32].

Eq. (11) describes a limiting case since its accounts for a significant decrease in the permeability when the alloy is saturated with hydrogen. The results of test calculations of heat-and-mass transfer (see Fig. S3 in the *Supplementary information*) were shown to be non-sensitive to the permeability value for the reactor design under consideration.

As a result, the effective thermal conductivity is the main parameter which determines dynamics of hydrogen absorption/desorption. In this work, we model the effective thermal conductivity as presented in Refs. [41,42]:

$$\lambda_{eff} = \frac{1}{1 + 2Kn\frac{2-a}{a}} \bullet \frac{\lambda_g}{\varphi^3} + \lambda_{eff,0} \tag{12}$$

$$Kn = \frac{\bar{l}}{\sqrt{k}} = \frac{(1 - \varphi)k_b T_s}{10\sqrt{3}\,\varphi\,p_{H_2}\pi\,r_{H_2}^2} \tag{13}$$

where Kn is the Knudsen number, k_b is the Boltzmann constant; r_{H2} is the radius of H_2 molecule; a is an empiric coefficient, the value $a = 0.55$ and $\lambda_{eff,0} = 3.7 \bullet 10^{-3}$ W/(m K) were selected on the basis of experimental data [30]; $\lambda_{eff,0}$ is the effective thermal conductivity of the MH bed in vacuum.

If to neglect the Knudsen effect, the only parameters necessary for the calculation of the effective thermal conductivity of the MH bed will be thermal conductivity of the filling gas and the bed porosity. There exist more detailed models, e.g., the one presented in Ref. [31] by the authors who collected the corresponding experimental data [30]. The model [31] takes into account the changes of contact area of the MH particles during hydrogen absorption. However, it requires a big number of the input parameters. Fig. S4 in the Supplementary Information presents a comparison of the calculation results according to the model used in our work and the model [31]. It is seen that both models yield similar results and reproduce well enough the experimental data for the MH beds with different porosities and the mean particle sizes.

Fig. S5 in the *Supplementary Information* presents dependence of the effective thermal conductivity of the MH bed on the basis of LaNi$_5$ on the hydrogen saturation fraction. It is seen that both the model used in our work and the model [31] yield similar results.

When using two-temperature model, the effective thermal conductivity of the gas phase, λ_g^*, was assumed to be equal to thermal conductivity of hydrogen, λ_g, the effective thermal conductivity of the solid, λ_s^*, was determined from Eq. (14) valid in the one-temperature approximation:

$$\lambda_s^* = \frac{\lambda_{eff} - \varphi\,\lambda_g^*}{1 - \varphi} \tag{14}$$

The presented model, as to its applicability for the simulation of heat-and-mass transfer in MH beds with unchanged properties, was validated in Refs. [21,42–44]. The details of the in-house developed CFD code "ANES" used in the simulation were described in Ref. [21]. The features of the temporal and spatial discretisation of the task and the results of grid independency tests are presented in *Supplementary Information, Section S1*.

3. Results and discussion

3.1. Modelling approaches

Hydrogen absorption and desorption were modelled using various approaches to the determination of the MH bed properties. The parameters of the simulated modes are presented in Table 1.

The approaches to the modelling of the MH bed properties during simulation are summarised in Table 2. For example, the abbreviation "Abs-3" means the simulation of the absorption mode using approach 3.

3.2. Hydrogen absorption

The modelling results obtained when using basic approaches to hydrogen absorption (Abs-1 and Abs-2) are presented in Fig. 2.

It is seen from Fig. 2 that the experimental data [34] are in between the modelling results obtained using approaches Abs-1 (constant porosity) and Abs-2 (variable porosity). Accounting $\varphi = \varphi(X)$ and $\rho_s = \rho_s(X)$ (Abs-2) results in the faster cooling of the MH bed due to increase of the effective thermal conductivity when the porosity decreases.

Since the procedure presented in Ref. [34] does not foresee the measurements of the input H$_2$ flow rate during absorption, Fig. 3 presents results of its simulation only, without comparison with the experimental data. Most probably, the experimental data are somewhere in between the two curves shown in Fig. 3. Note that on the first look the difference between the hydrogen absorption dynamics is insignificant, especially, taking into account low precision of the input data (e.g., the bed porosity). However, due to exponential nature of the curves, the times of achievement $X = 0.9$ differ significantly: 31.1 min for Abs-1 and 22.1 min for Abs-2.

The time dependencies of the effective thermal conductivity, hydrogen-saturated fraction of the alloy, the bed porosity and the material density in the point A during H$_2$ absorption are shown in the

Table 1
The simulated modes.

Abbreviation	Operation mode	Input/output boundary condition	Cooling/ heating conditions	Initial conditions
Abs	Hydrogen absorption	Constant pressure ($p = 8$ bar)	$T = 20°C$; $\alpha = 1650$ W/ (m^{2}K)	$T = 20°C$; $X = 0.04$
Des	Hydrogen desorption	Constant output flow rate (from 0.5 to 2.0 Nl/min)	$T = 60°C$; $\alpha = 1650$ W/ (m^{2}K)	$p = 8$ bar; $X = 0.94$

Table 2
Approaches to the modelling of MH bed properties.

| Approach number (e.g., Abs-1, Des-2, etc.)	Porosity, φ Density, ρ	Effective thermal conductivity, λ_{eff}	Comment
1	$\varphi = \varphi_{X=0}$ $\rho_s = \rho_{s,X=0}$	Eq. (12)	Base variant of the calculation assuming the constant porosity
2	$\varphi = \varphi(X)$ $\rho_s = \rho_s(X)$	Eq. (12)	Base variant of the calculation assuming the variable porosity
3	$\varphi = \varphi(X)$ $\rho_s = \rho_s(X)$	$\lambda_{eff} = 0.86 + 0.235 \bullet X$	Linear dependence $\lambda_{eff}(X)$; the coefficients were fitted towards the best correspondence of the calculation results and the experimental data [34] on the dynamics of temperature changes
4	$\varphi = \varphi(X)$ $\rho_s = \rho_s(X)$	$\lambda_{eff} = 1.32$ W/ (m·K)	The constant value of λ_{eff} was fitted towards achievement of the same absorption time from $X = 0.04$ to $X = 0.9$ when applying approaches Abs-2 and Abs-4
5	$\varphi = \varphi(X)$ $\rho_s = \rho_s(X)$	$\lambda_{eff} = 0.89$ W/ (m·K)	The constant value of λ_{eff} was fitted towards achievement of the same dynamics of the pressure change in the MH reactor during desorption at the constant flow rate when applying approaches Des-2 and Des-5
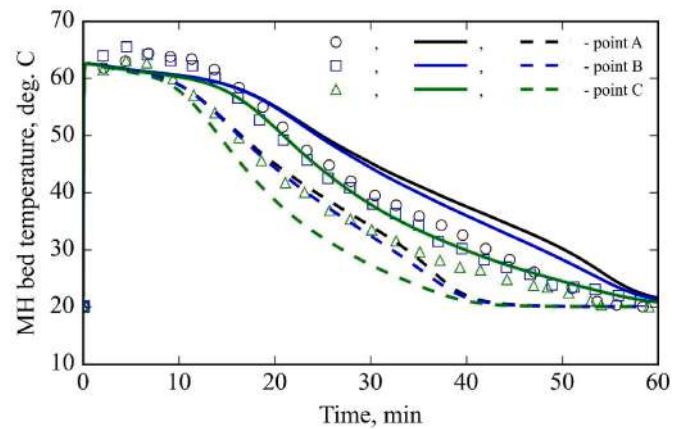
Fig. 2. Changes of the MH bed temperature in points A, B and C of the MH reactor (Fig. 1) during hydrogen absorption. Points – experimental data [34]. Solid lines – modelling (Abs-1). Dashed lines – modelling (Abs-2).

Supplementary Information; Figs. S6 and S7. Due to decrease of the material density and the corresponding decrease of the bed porosity, the effective thermal conductivity increases from 0.86 to 1.4 W/(m K) that corresponds well to the ranges of values presented in the literature [29, 31,34,45,46].

Figs. 4–6 present colour maps of the fields of temperature, hydrogen-saturated fraction of the alloy and the effective thermal conductivity of the MH bed at different times.

It is seen from Figs. 4–6 that the absorption reaction propagates as a front moving from the reactor wall to its centre. The heat from the region of the active absorption is transferred via the hydrogen-saturated region characterised by the higher effective thermal conductivity.

It is possible to estimate the "real" changes of the effective thermal conductivity. Let's assume the following dependence:
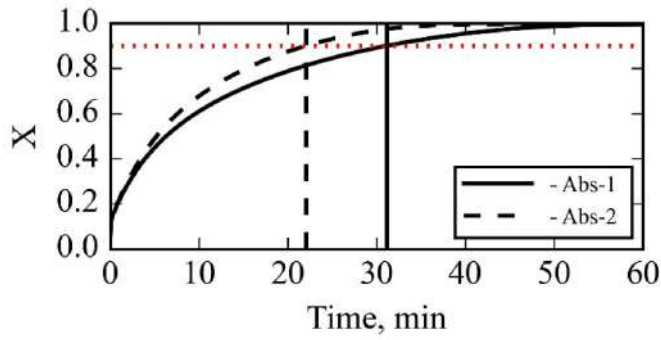
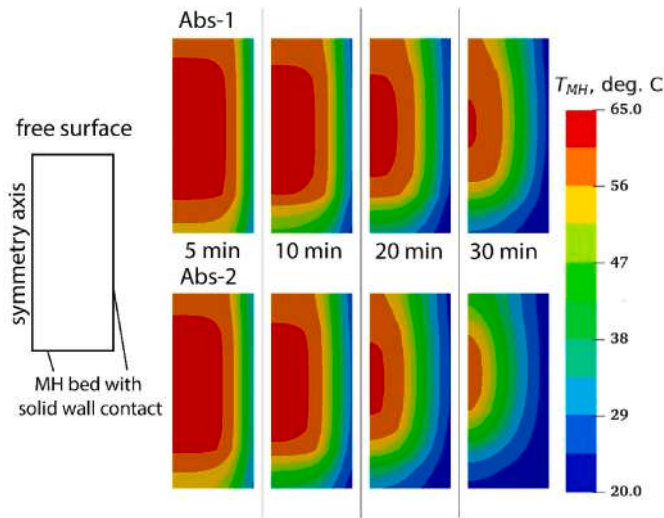**Fig. 3.** Simulated dynamics of hydrogen absorption.

Fig. 4. Temperature fields calculated according to the modelling approaches Abs-1 and Abs-2.

$$\lambda_{eff} = \lambda_{eff}(X=0) + \Delta\lambda_{eff} \bullet X \qquad (15)$$

where $\Delta\lambda_{eff}$ is the specific change of the effective thermal conductivity during H_2 absorption. The starting value $\lambda_{eff}(X=0)$ was assumed to be equal to 0.86 W/(m K), i.e., the value calculated at $X = 0$ by applying the model of the effective thermal conductivity used in our work. The value of $\Delta\lambda_{eff}$ was fitted using in-house developed Python code which minimised the deviation of the calculated and experimentally observed dynamics of the temperature changes in the points A, B and C of the MH reactor (Fig. 1). The fitted value $\Delta\lambda_{eff} = 0.235$ W/(m K) was used during calculations according to Eq. (15) using approach Abs-3 (Tables 1 and 2).

A comparison of the dynamics of temperature changes modelled using approaches Abs-2 and Abs-3 is presented in Fig. 7. The better correspondence between the experimental data and the calculations which assume the smaller changes of the effective thermal conductivity (Abs-3) is explained by the limiting nature of the Abs-2 approach. However, in the reality, the bed porosity changes in a lesser extent due to presence of a free volume above the bed (see updated task statement in the Supplementary Information, Fig. S8).

The above effect was accounted in this study by assuming that the hydrogen absorption takes place at a constant effective thermal conductivity whose value provides the same H_2 absorption dynamics as during the absorption at variable porosity. The coincidence (see Fig. S9 in the Supplementary Information) was achieved at the fitted value λ_{eff} = 1.32 W/(m·K). Same dynamics of the H_2 absorption assuming the variable (model Abs-2) and the constant (model Abs-4) effective thermal
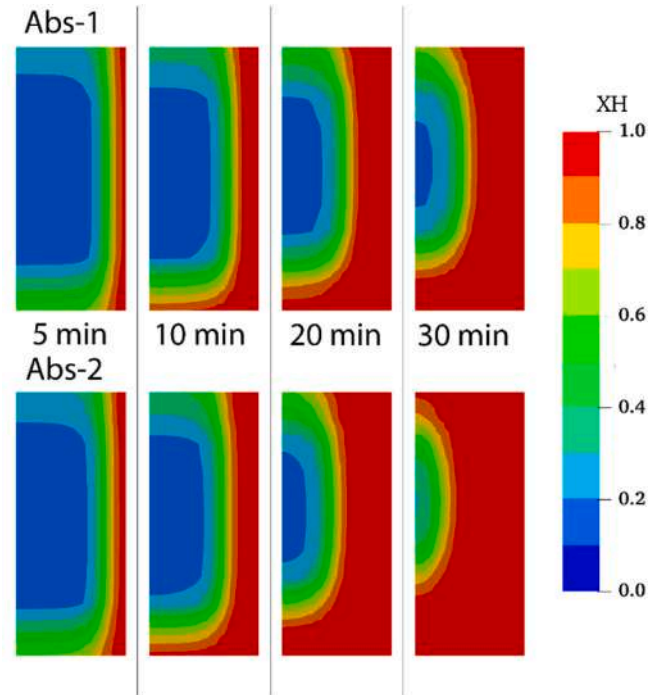

Fig. 5. Fields of hydrogen-saturated fraction of the alloy calculated according to the modelling approaches Abs-1 and Abs-2.
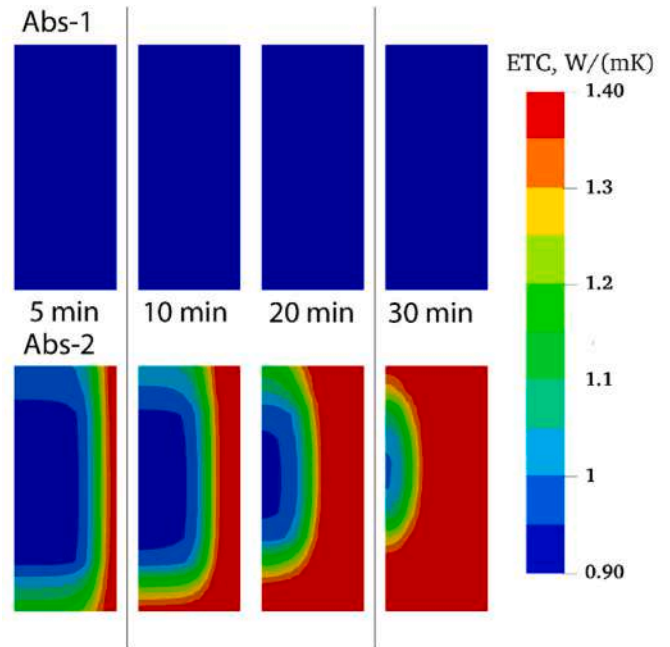

Fig. 6. Fields of the effective thermal conductivity calculated according to the modelling approaches Abs-1 and Abs-2.

conductivity has its origin in the fact that the alloy in proximity to the reactor wall absorbs hydrogen faster than the alloy located closer to the axis (Figs. 4, 5 and 8). This nonuniformity results in the heat transfer mostly through the hydrogen-saturated zone of the MH bed characterised by the higher value of λ_{eff} than the non-saturated zone.

3.3. Hydrogen desorption

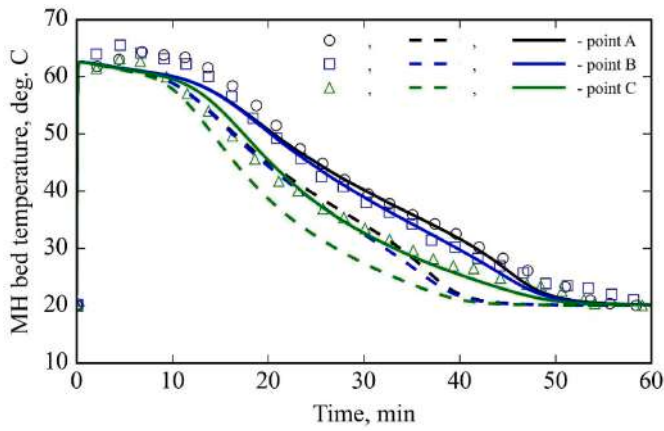The changes of the effective thermal conductivity have the most

Fig. 7. Comparison of the calculation results according to the models Abs-2 (dashed lines) and Abs-3 (solid lines) with the experimental data [34] (points).

significant influence on the hydrogen desorption behaviour at a constant flow rate. When the desorption takes place, the effective thermal conductivity decreases resulting in the increase of temperature difference between the bed and the heating fluid. In doing so, hydrogen pressure in the reactor decreases faster, to provide hydrogen desorption dynamics which maintains the pre-set hydrogen flow rate.

The results of H_2 desorption modelling which assumes variable effective thermal conductivity (model Des-2) or the constant thermal conductivity of 1.32 W/(m K) providing the same dynamics of H_2 absorption (model Des-4) are presented in Fig. 9. The figure shows changes of hydrogen pressure in the reactor for three values of the output flow rates: 0.5, 1.0 and 2.0 Nl/min. It is seen that the error in the predicted time of supplying H_2 at the pre-set flow rate until pressure drop below 1 bar (horizontal line) can be as high as 20%.

Similarly to introducing the model Abs-4 (see the corresponding comments in Section 3.2), we fitted the constant value of the effective thermal conductivity equal to 0.89 W/(m K) at which the dynamics of the pressure changes in the MH reactor at the maximum H_2 output flow rate of 2 Nl/min was the same as for the calculations according to the model Des-2. The low value of λ_{eff} close to the one for the bed non-saturated with hydrogen is explained by the fast H_2 desorption from the zone close to the reactor wall and, in turn, having low effective thermal conductivity (Fig. 10).

The results of H_2 desorption modelling which assumes variable effective thermal conductivity (model Des-2) or the constant thermal conductivity of 0.89 W/(m K) (model Des-5) are presented in Fig. 11.

It is seen that the use of constant value of ETC predicts well the initial stage of the desorption for all flow rates and completely reproduces the mode at the maximum flow rate for which the used constant ETC value was fitted. Minor differences for the lower flow rates at the end of desorption have their origin in the contribution of Knudsen effects at the

lower pressures into the influence of hydrogen concentration (X) on the ETC.

3.4. Discussion

The changes of density of the solid phase of the MH bed during hydrogen absorption (decrease) and desorption (increase) result in the corresponding decrease/increase of the bed porosity and, in turn, increase/decrease of its effective thermal conductivity. It significantly affects results of the modelling of heat-and-mass transfer in MH reactor.

Presently, the effect considered in this work can be studied in only idealised statement, i.e., without accounting for the presence of a free volume above the MH bed. The reason is not in a more complicated procedure of the modelling of a deformed porous medium but, first of all, in the increase of the number of the poorly controlled in the experiment input parameters which are necessary to close the model. It can be confirmed, for example, by the work [47] where a detailed mathematical model describing thermo-mechanics of a MH reactor was presented. Because of diversity of the possible arrangements of the MH bed in the reactor, significant changes of the bed structure during the period from the loading in the reactor to the end of activation, changes of particle size distribution along the height of the reactor due to cyclic swelling/shrinking of the MH bed [48], as well as relatively small number of publications which consider practically important mode of desorption with the constant flow rate [35,49], some effects could be studied rather qualitatively than quantitatively. To improve the situation, it is necessary to carry out experiments in which the state of the MH bed is carefully monitored not only before its loading into MH reactor but also during its operation (see Ref. [50] as example).
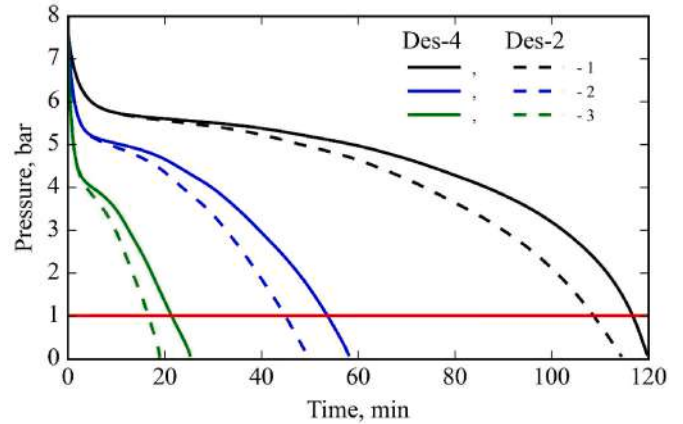

Fig. 9. Results of calculations according to the models Des-2 and Des-4 of hydrogen pressure in the MH reactor during desorption at the constant H_2 output flow rates of 0.5 (1), 1.0 (2) and 2.0 Nl/min (3).
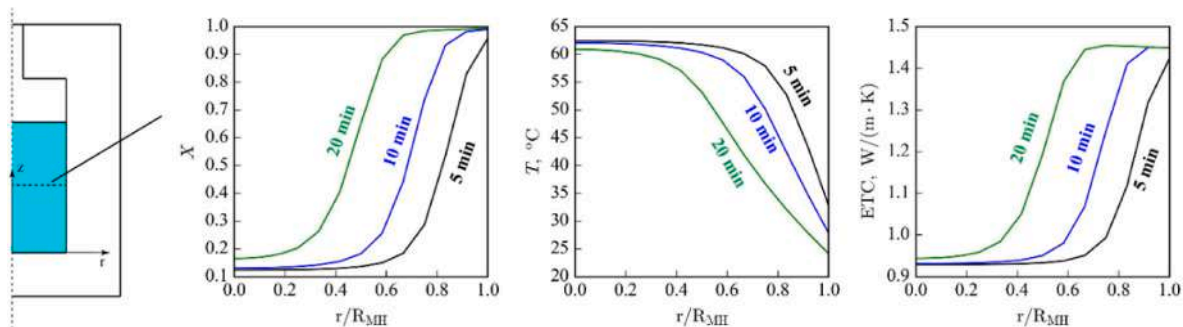

Fig. 8. Radial distributions of the hydrogen-saturated fraction, temperature, and effective thermal conductivity of the MH bed during hydrogen absorption.
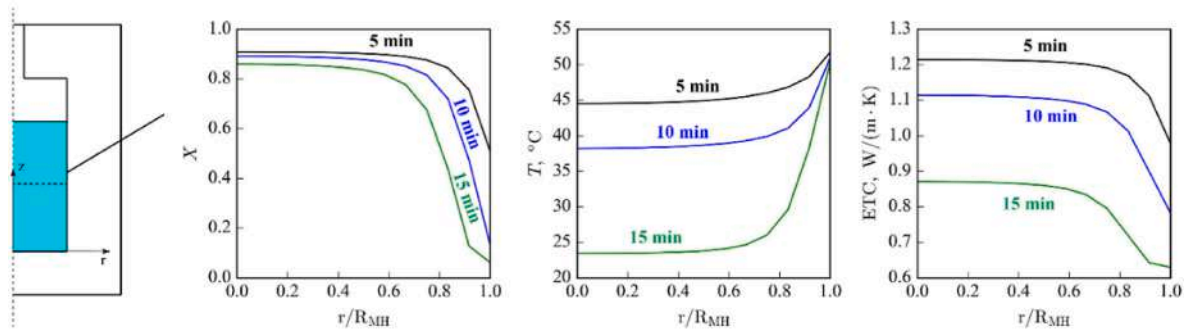
Fig. 10. Radial distributions of the hydrogen-saturated fraction, temperature, and effective thermal conductivity of the MH bed during hydrogen desorption.
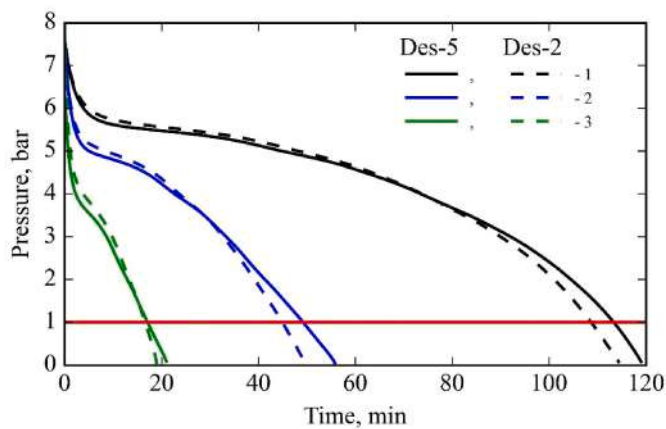

Fig. 11. Results of calculations according to the models Des-2 and Des-5 of hydrogen pressure in the MH reactor during desorption at the constant H_2 output flow rates of 0.5 (1), 1.0 (2) and 2.0 Nl/min (3).

The idealised schematics of hydrogen absorption/desorption behaviour is shown in Fig. 12. The absorption/desorption front moves from the cooled/heated reactor wall towards the axis of the cylindrical reactor. The zone of the MH bed near the wall quickly becomes saturated with hydrogen (absorption) or hydrogen-depleted (desorption) that results in the increase or decrease, respectively, of its effective thermal conductivity. The heat released/absorbed in the region of active H_2 absorption/desorption, closer to the axis of the reactor, is released/supplied trough the reactor periphery.

Accordingly, during H_2 absorption the heat release will be rate-limited by the effective thermal conductivity of hydrogen-saturated MH bed which has to be taken for the modelling. Conversely, during H_2 desorption the heat supply will be rate-limited by the effective thermal conductivity of the hydrogen-depleted bed, and for correct simulation of heat-and-mass transfer for H_2 desorption the latter value should be taken as the input parameter.

4. Conclusions and recommendations

- Accounting of the real changes of density of hydrogen storage material during H_2 absorption and desorption may result in the significant changes of porosity of the metal hydride bed and, in turn, changes of its effective thermal conductivity.
- This work has considered a limiting case when the volume of the metal hydride bed does not change. In the reality, due to the bed deformation and the change of its volume, the porosity decrease during H_2 absorption may be smaller to result in the better agreement of experimental data and the calculation results.
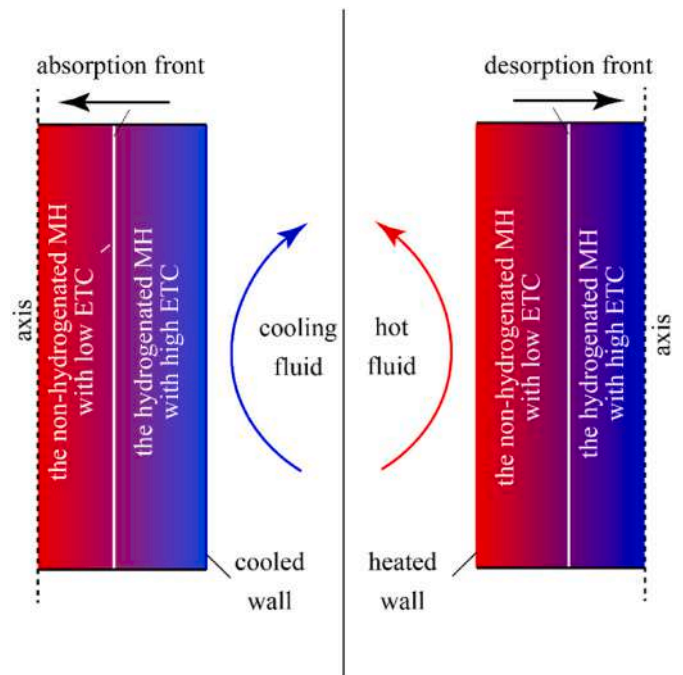

Fig. 12. Idealised schematics of H_2 absorption/desorption processes in a cylindrical reactor with external heating and cooling.

- There is a lack of the precise experimental data in the literature for the model validation.
- The modelling of desorption modes at the constant and variable value of the bed porosity showed a noticeable difference in the estimation of the time during which the system can supply hydrogen at the constant flow rate and pre-defined H_2 pressure.
- When carrying out the absorption modelling assuming the constant effective thermal conductivity, it is recommended to use the value which corresponds to the hydrogen-saturated metal hydride bed.
- When modelling desorption, it is better to use the value of the effective thermal conductivity which corresponds to the hydrogen-depleted metal hydride bed.

CRediT authorship contribution statement

Konstantin B. Minko: Formal analysis, Investigation, Methodology, Software, Validation, Writing – original draft. **Mykhaylo V. Lototskyy:** Conceptualization, Formal analysis, Resources, Supervision, Writing – review & editing, Funding acquisition. **Irina E. Bessarabskaya:** Formal analysis, Investigation, Visualization. **Boris P. Tarasov:** Funding acquisition, Project administration, Resources.

Declaration of competing interest

The authors declare that they have no known competing financial interests or personal relationships that could have appeared to influence the work reported in this paper.

Acknowledgements

Appendix A. Supplementary data

Supplementary data to this article can be found online at https://doi.org/10.1016/j.ijhydene.2024.05.083.

References

[1] Rivard E, Trudeau M, Zaghib K. Hydrogen storage for mobility: a review. Materials 2019;12:1973. https://doi.org/10.3390/ma12121973.

[2] Pistidda C. Solid-state hydrogen storage for a decarbonized society. Hydro 2021;2:428–43. https://doi.org/10.3390/hydrogen2040024.

[3] Amirthan T, Perera MSA. The role of storage systems in hydrogen economy: a review. J Nat Gas Sci Eng 2022;108. https://doi.org/10.1016/j.jngse.2022.104843.

[4] Usman MR. Hydrogen storage methods: review and current status. Renew Sustain Energy Rev 2022;167. https://doi.org/10.1016/j.rser.2022.112743.

[5] Muhammed NS, Gbadamosi AO, Epelle EI, Abdulrasheed AA, Haq B, Patil S, et al. Hydrogen production, transportation, utilization, and storage: recent advances towards sustainable energy. J Energy Storage 2023;73:109207. https://doi.org/10.1016/j.est.2023.109207.

[6] Ge L, Zhang B, Huang W, Li Y, Hou L, Xiao J, et al. A review of hydrogen generation, storage, and applications in power system. J Energy Storage 2024;75:109307. https://doi.org/10.1016/j.est.2023.109307.

[7] Irham A, Roslan MF, Jern KP, Hannan MA, Mahlia TMI. Hydrogen energy storage integrated grid: a bibliometric analysis for sustainable energy production. Int J Hydrogen Energy 2024;63:1044–87. https://doi.org/10.1016/j.ijhydene.2024.03.235.

[8] Bosu S, Rajamohan N. Recent advancements in hydrogen storage - comparative review on methods, operating conditions and challenges. Int J Hydrogen Energy 2024;52:352–70. https://doi.org/10.1016/j.ijhydene.2023.01.344.

[9] Lin A, Bagnato G. Revolutionising energy storage: the Latest Breakthrough in liquid organic hydrogen carriers. Int J Hydrogen Energy 2024;63:315–29. https://doi.org/10.1016/j.ijhydene.2024.03.146.

[10] Nivedhitha KS, Beena T, Banapurmath NR, Umarfarooq MA, Ramasamy V, Soudagar MEM, et al. Advances in hydrogen storage with metal hydrides: mechanisms, materials, and challenges. Int J Hydrogen Energy 2024;61:1259–73. https://doi.org/10.1016/j.ijhydene.2024.02.335.

[11] Lototskyy MV, Tolj I, Pickering L, Sita C, Barbir F, Yartys V. The use of metal hydrides in fuel cell applications. Prog Nat Sci: Mater Int 2017;27. https://doi.org/10.1016/j.pnsc.2017.01.008.

[12] Hirscher M, Yartys VA, Baricco M, Bellosta von Colbe J, Blanchard D, Bowman RC, et al. Materials for hydrogen-based energy storage – past, recent progress and future outlook. J Alloys Compd 2020;827:153548. https://doi.org/10.1016/j.jallcom.2019.153548.

[13] Cetinkaya SA, Disli T, Soyturk G, Kizilkan O, Colpan CO. A review on thermal coupling of metal hydride storage tanks with fuel cells and electrolyzers. Energies 2022;16:341. https://doi.org/10.3390/en16010341.

[14] Lototskyy MV, Tarasov BP, Yartys VA. Gas-phase applications of metal hydrides. J Energy Storage 2023;72:108165. https://doi.org/10.1016/j.est.2023.108165.

[15] Sreeraj R, Aadhithiyan AK, Anbarasu S. Integration of thermal augmentation methods in hydride beds for metal hydride based hydrogen storage systems: review and recommendation. J Energy Storage 2022;52:105039. https://doi.org/10.1016/j.est.2022.105039.

[16] Kukkapalli VK, Kim S, Thomas SA. Thermal management techniques in metal hydrides for hydrogen storage applications: a review. Energies 2023;16:3444. https://doi.org/10.3390/en16083444.

[17] Jiao K, Li X, Yin Y, Zhou Y, Yu S, Du Q. Effects of various operating conditions on the hydrogen absorption processes in a metal hydride tank. Appl Energy 2012;94:257–69. https://doi.org/10.1016/j.apenergy.2012.01.033.

[18] Zhuo Y, Jung S, Shen Y. Numerical study of hydrogen desorption in an innovative metal hydride hydrogen storage tank. Energy & Fuels 2021;35:10908–17. https://doi.org/10.1021/acs.energyfuels.1c00666.

[19] Akanji O, Kolesnikov AV. Modelling of hydrogen adsorption/desorption in metal hydride reactor. J Comput Theor Nanosci 2010;7:2112–5. https://doi.org/10.1166/jctn.2010.1592.

[20] Raju M, Kumar S. Optimization of heat exchanger designs in metal hydride based hydrogen storage systems. Int J Hydrogen Energy 2012;37:2767–78. https://doi.org/10.1016/j.ijhydene.2011.06.120.

[21] Minko KB, Bocharnikov MS, Yanenko YB, Lototskyy MV, Kolesnikov A, Tarasov BP. Numerical and experimental study of heat-and-mass transfer processes in two-stage metal hydride hydrogen compressor. Int J Hydrogen Energy 2018:21874–85. https://doi.org/10.1016/j.ijhydene.2018.09.211.

[22] Nashchekin MD, Minko KB, Artemov VI. Numerical analysis of constructive and regime parameter effects on the efficiency of metal hydride systems for hydrogen purification. Case Stud Therm Eng 2019;14:100485. https://doi.org/10.1016/j.csite.2019.100485.

[23] Chibani A, Merouani S, Bougriou C. The performance of hydrogen desorption from a metal hydride with heat supply by a phase change material incorporated in porous media (metal foam): heat and mass transfer assessment. J Energy Storage 2022;51:104449. https://doi.org/10.1016/j.est.2022.104449.

[24] Mohammadshahi SS, Gray EMacA, Webb CJ. A review of mathematical modelling of metal-hydride systems for hydrogen storage applications. Int J Hydrogen Energy 2016;41:3470–84. https://doi.org/10.1016/j.ijhydene.2015.12.079.

[25] Chabane D, Harel F, Djerdir A, Ibrahim M, Candusso D, Elkedim O, et al. Influence of the key parameters on the dynamic behavior of the hydrogen absorption by LaNi5. Int J Hydrogen Energy 2017;42:1412–9. https://doi.org/10.1016/j.ijhydene.2016.06.110.

[26] Griessen R, Feenstra R. Volume changes during hydrogen absorption in metals. J Phys F Met Phys 1985;15:1013–9. https://doi.org/10.1088/0305-4608/15/4/024.

[27] Gillia O. Hydride breathing and its consequence on stresses applied to containers: a review. Int J Hydrogen Energy 2021;46:35594–640. https://doi.org/10.1016/j.ijhydene.2021.07.082.

[28] Matsushita M, Monde M, Mitsutake Y. Predictive calculation of the effective thermal conductivity in a metal hydride packed bed. Int J Hydrogen Energy 2014;39:9718–25. https://doi.org/10.1016/j.ijhydene.2014.04.072.

[29] Mellouli S, Askri F, Dhaou H, Jemni A, Ben Nasrallah S. A study of the thermal behavior of a deformable metal-hydride bed. Int J Hydrogen Energy 2016;41:1711–24. https://doi.org/10.1016/j.ijhydene.2015.10.058.

[30] Hahne E, Kallweit J. Thermal conductivity of metal hydride materials for storage of hydrogen: experimental investigation. Int J Hydrogen Energy 1998;23:107–14. https://doi.org/10.1016/S0360-3199(97)00020-7.

[31] Kallweit J, Hahne E. Effective thermal conductivity of metal hydride powders: measurement and theoretical modelling. In: Proceeding of international heat transfer conference 10, Connecticut: begellhouse; 1994. p. 373–8. https://doi.org/10.1615/IHTC10.790.

[32] Mitsutake Y, Monde M, Tanaka S, Miura S, Fujisawa A. Measurement of gas permeability for MH-Fe particle mixture column bed. Journal of the Hydrogen Energy Systems Society of Japan 2012;37:262–7. https://doi.org/10.50988/hess.37.3_262.

[33] Dunikov DO, Blinov DV, Bozieva AM, Kazakov AN, Krapivina AA, Romanov IA, et al. Permeability of a deformable metal hydride bed during hydrogen absorption. Int J Hydrogen Energy 2024;51:375–87. https://doi.org/10.1016/j.ijhydene.2023.05.224.

[34] Jemni A, Ben Nasrallah S, Lamloumi J. Experimental and theoretical study of a metal–hydrogen reactor. Int J Hydrogen Energy 1999;24:631–44. https://doi.org/10.1016/S0360-3199(98)00117-7.

[35] Andreasen G, Melnichuk M, Ramos S, Corso HL, Visintin A, Triaca WE, et al. Hydrogen desorption from a hydride container under different heat exchange conditions. Int J Hydrogen Energy 2013;38:13352–9. https://doi.org/10.1016/j.ijhydene.2013.07.115.

[36] Villars P, editor. Springer materials: LaNi5 crystal structure. PAULING FILE in: inorganic solid phases. SpringerMaterials (Online Database); 2023. https://materials.springer.com/isp/crystallographic/docs/sd_0251595. [Accessed 20 December 2023].

[37] Villars P, editor. Springer materials: LaNi5H6 (LaNi5H5.7) crystal structure. PAULING FILE in: inorganic solid phases. SpringerMaterials (Online Database); 2023. https://materials.springer.com/isp/crystallographic/docs/sd_0306625. [Accessed 20 December 2023].

[38] Pons M, Dantzer P. Heat transfer in hydride packed beds. II. A new experimental technique and results on LaNi5 powder. Z Phys Chem 1994;183:213–23. https://doi.org/10.1524/zpch.1994.183.Part_1_2.213.

[39] Minko KB, Artemov VI, Yan'kov GG. Numerical simulation of sorption/desorption processes in metal-hydride systems for hydrogen storage and purification. Part I: development of a mathematical model. Int J Heat Mass Tran 2014;68:683–92. https://doi.org/10.1016/j.ijheatmasstransfer.2013.09.056.

[40] Mayer U, Groll M, Supper W. Heat and mass transfer in metal hydride reaction beds: experimental and theoretical results. Journal of the Less Common Metals 1987;131:235–44. https://doi.org/10.1016/0022-5088(87)90523-6.

[41] Artemov VI, Lazarev DO, Yan?kov GG, Borzenko VI, Dunikov DO, Malyshenko SP. The effect of non-absorbable gas impurities on heat and mass transfer in metal-hydride devices for storage and purification of hydrogen. High Temp 2004;42:987–95. https://doi.org/10.1007/s10740-005-0021-8.

[42] Minko KB, Nashchekin M. Thermal performance of a metal hydride reactor for hydrogen storage with cooling/heating by natural convection. Energy Storage and Saving 2023;2:597–607. https://doi.org/10.1016/j.enss.2023.08.006.

[43] Minko KB, Artemov VI, Yan'kov GG. Numerical simulation of sorption/desorption processes in metal-hydride systems for hydrogen storage and purification. Part II: verification of the mathematical model. Int J Heat Mass Tran 2014;68:693–702. https://doi.org/10.1016/j.ijheatmasstransfer.2013.09.057.

[44] Minko K. Commentary on "A continuous hydrogen absorption/desorption model for metal hydride reactor coupled with PCM as heat management and its application in the fuel cell power system". Int J Hydrogen Energy 2022;47:10799–801. https://doi.org/10.1016/j.ijhydene.2021.12.231 [Yao J, Zhu P, Guo

L, Duan L, Zhang Z, Kurko S et al. Int J Hydrogen Energy 2020. 10.1016/j. ijhydene.2020.05.089].

[45] Yoshida A, Naka Y, Ohkita T. Experimental study on thermophysical and kinetic properties of the LaNi5-H2 system. TRANSACTIONS OF THE JAPAN SOCIETY OF MECHANICAL ENGINEERS Series B 1990;56:536–40. https://doi.org/10.1299/kikaib.56.536.

[46] Nakagawa T. Numerical analysis of heat and mass transfer characteristics in the metal hydride bed. Int J Hydrogen Energy 2000;25:339–50. https://doi.org/10.1016/S0360-3199(99)00036-1.

[47] Lexcellent C, Gay G, Chapelle D. Thermomechanics of a metal hydride-based hydrogen tank. Continuum Mech Therm 2015;27:379–97. https://doi.org/10.1007/s00161-014-0356-7.

[48] Lin X, Sun D, Chen S, Zhu Q, Leng H, Li Q. Numerical analysis on pulverization and self-densification for hydrogen storage performance of a metal hydride tank. Appl Therm Eng 2019;161:114129. https://doi.org/10.1016/j.applthermaleng.2019.114129.

[49] Yao J, Zhu P, Guo L, Duan L, Zhang Z, Kurko S, et al. A continuous hydrogen absorption/desorption model for metal hydride reactor coupled with PCM as heat management and its application in the fuel cell power system. Int J Hydrogen Energy 2020;45:28087–99. https://doi.org/10.1016/j.ijhydene.2020.05.089.

[50] Borzenko VI, Romanov IA, Dunikov DO, Kazakov AN. Hydrogen sorption properties of metal hydride beds: effect of internal stresses caused by reactor geometry. Int J Hydrogen Energy 2019;44:6086–92. https://doi.org/10.1016/j.ijhydene.2019.01.052.